Understanding the interplay of transport-morphology-performance in PBDB-T based polymer solar cells

Qilin Zhang, Xin Yuan, Yifeng Feng, Bryon W. Larson, Gregory M. Su, Yin Maung Maung, Nopporn Rujisamphan, Youyong Li, Jianyu Yuan, Wanli Ma**

Qilin Zhang, Xin Yuan, Yifeng Feng, Prof. Youyong Li, Prof. Jianyu Yuan, Prof. Wanli Ma
Institute of Functional Nano & Soft Materials (FUNSOM), Jiangsu Key Laboratory for Carbon-Based Functional Materials and Devices, Joint International Research Laboratory of Carbon-Based Functional Materials and Devices, Soochow University, Suzhou, 215123, P. R. China, Email: jyyuan@suda.edu.cn; wlma@suda.edu.cn

Dr. Bryon W. Larson
Chemistry & Nanoscience Department, National Renewable Energy Laboratory, Golden, Colorado 80401, United States

Dr. Gregory M. Su
Advanced Light Source, Lawrence Berkeley National Laboratory, Berkeley, California 94720, United States

Prof. Yin Maung Maung,
Department of Physics, University of Yangon, Pyay Road, Yangon 11181, Myanmar

Prof. Nopporn Rujisamphan
King Mongkut's University of Technology Thonburi (KMUTT), 126 Pracha Uthit Road, Bang Mod, Thung Khru, Bangkok 10140, Thailand

Keywords: polymer solar cells, nonfullerene acceptor, time-resolved microwave conductivity (TRMC), free carrier mobility, stability

Abstract: Polymer-polymer blends have been reported to exhibit exceptional thermal and ambient stability. However, power conversion efficiencies (PCEs) from devices using polymeric acceptors have been recorded to be significantly lower than those based on conjugated molecular acceptors. Here, two organic nonfullerene bulk heterojunction (BHJ) blends ITIC:PBDB-T and N2200:PBDB-T, together with their fullerene counterpart, PCBM:PBDB-T, are adopted to understand the effect of electron acceptors on device performance. We comprehensively investigate free charge carrier properties using time-resolved microwave conductivity (TRMC) measurements. The nonfullerene devices show an improved PCE of 10.06% and 6.65% in the ITIC and N2200 based cells, respectively. In

comparison, the PCBM: PBDB-T based devices yielded a PCE of 5.88%. The optimal N2200: PBDB-T produced the highest TRMC mobility, longest lifetime, and greatest free carrier diffusion length. We found that such phenomena can be associated with the unfavorable morphology of the all-polymer BHJ microstructure. In contrast, the solar cell using either the PCBM or ITIC acceptors display a more balanced donor and acceptor phase separation, leading to more efficient free carrier separation and transport in an operating device. Sacrificing efficiency for superior stability, we show that the improved structure in all-polymer blend could deliver a more stable morphology under thermal stress.

1. Introduction

Polymer solar cells (PSCs), which are composed of a polymeric donor and an electron acceptor (fullerene molecule, conjugated small molecule, conjugated polymer or mixed)[1-5] exhibit great potential for solution-processed next-generation solar cells. By adjusting the chemical structure of the donor material,[6-7] conjugated polymers can exhibit extended absorption and higher hole mobilities. In 2014, polymer-fullerene solar cells obtained a certified power conversion efficiency (PCE) of over 10%.[8-9] Over the past 5 years, great success has been achieved in polymeric solar cells adopting nonfullerene electron acceptors,[3-5] with PCEs now exceeding 16.0%.[10-11] Nonfullerene molecular or polymeric electron acceptors offer unique opportunities for photovoltaic applications due to their flexible structure tunability and new device features that emerge at the donor/acceptor heterojunction. Besides, the adoption of nonfullerene materials can offer exceptional stability which has not been achieved in previous polymer-fullerene systems.[12-14] This progression demonstrates the potential for nonfullerene polymer solar cells and its advantages for further design opportunities for efficient and stable solar cells for large-scale applications.

Incorporation of nonfullerene acceptors can extend the solar cell photoresponse to over 800 nm using a wide bandgap donor polymer.[3-4] Conjugated molecules and polymers tend to

exhibit better thermal stability than conventional fullerene derivatives. This property presents unique potential as these materials are less prone to thermal stress and possess better phase stability.[14-16] However, the morphology of bulk heterojunction (BHJ) blend film is detrimental to charge transport and recombination. Therefore, the adoption of processing additives has become a conventional optimization technique and effectatively alter the active layer morphology.[17] In general, these additives usually have a high boiling point and possess selective solubility to one of the active materials. [18] However, the addition of these additives usually work less efficient in either small moleculae and polymer based nonfullerne solar cells relative to the conventional polymer-fullerene based ones.[19] *Zhan et al.* first reported efficient nonfullerene solar cells using a newly designed conjugated molecular acceptor ITIC,[20] which outperforms conventional PCBM based devices. Meanwhile, the PCE of polymer-polymer (all-polymer) solar cells have also rapidly progressed and now exceed 11%.[21-23] Currently, PSC research is mainly focused on two aspects: exploring more solar-efficient materials with a focus on nonfullerene acceptors and device engineering to improve charge transport and recombination. Both efforts were dedicated to further improve the photovoltaic performance of the solar cell. However, less investigations have been carried out to explore the fundamental properties of these materials, which is important and helpful in understanding the current device performance as well as potentially providing guidelines to design novel materials and device architecture.

In this work, we comprehensively investigated the charge transport and photovoltaic performance of three representative organic BHJ solar cells: polymeric donor PBDB-T blended with PCBM, nonfullerene acceptor ITIC, and N2200[24] (also known as P(NDI2OD-T2)). The N2200:PBDB-T BHJ blend was fabricated under optimal conditions. Although it exhibited a mediocre PCE of 6.65%, it generated the highest free carrier mobility, lifetime, and the longest free carrier diffusion length. We found that such an imbalance between

photovoltaic performance and charge carrier properties can be attributed towards the blend

morphology. All-polymer blends show an unfavorable phase separation scale which further leads to increased charge recombination and thus decreases the solar-to-electricity conversion. nonetheless, solar cell devices based on the N2200:PBDB-T blend display excellent stability under thermal stress, which has been proven to be closely related to its "unique" morphology. We believe that these results will help understand the transport-morphology-performance relationship for efficient and stable polymer solar cells.

2. Results and Discussion

For consistency, all PSCs were fabricated with an inverted device architecture with a configuration of: indium-tin-oxide(ITO)/Zinc oxide (ZnO) /PBDB-T: Acceptor/MoO3/Ag, which is illustrated in **Figure 1**. The polymer PBDB-T and its derivatives are widely used as electron donors in recent organic solar cells.[3, 25] ITIC is considered as the pioneer of efficient nonfullerene acceptors, which opened a new door for further development of organic solar cells.[4] The polymer N2200 was first reported as an efficient n-type material for field-effect transistors[24] and has been recently adopted as an electron acceptor.[5,12] As shown in Figure S1, in comparison to the conventional PCBM acceptor, the absorption of both ITIC and N2200 polymers are well complemented with PBDB-T to cover the visible-to-NIR regions. The highest occupied molecular orbital (HOMO) of these materials were determined by ultraviolet photoelectron spectroscopy (UPS) characterization (Figure S2). As shown in **Figure 1**, the PBDB-T exhibits a HOMO level of -5.26 eV and the lowest unoccupied molecular orbital (LUMO) is calculated to be -3.46 eV. PCBM, ITIC, and N2200 exhibit a HOMO level of -5.92 eV, -5.71 eV, and -5.77 eV, respectively. Meanwhile, the LUMO level is calculated to be -4.10 eV, -4.13 eV, and -4.32 eV, respectively. Based on these results, all of these donor/acceptor combinations demonstrate favorable energy level alignments for achieving efficient charge separation.

As an initial study, we first compared the photovoltaic characteristics of the three representing BHJ systems. **Figure 2a** depicts the current density versus voltage (*J*-*V*) characteristics of the optimized PSCs using different electron acceptors under AM1.5G illumination at an intensity of 100 mW/cm^2. The devices fabricated with conventional PCBM exhibit an open-circuit voltage (V_{oc}) of 0.875 V, a short circuit current density (J_{sc}) of 10.34 mA/cm^2, a fill factor (FF) of 65.1%, and a best PCE of 5.88%. Fortunately, the strategy of employing nonfullerene acceptors takes advantage of improved absorption. ITIC:PBDB-T based devices exhibit a slightly higher V_{oc} of 0.910 V, a significantly improved J_{sc} of 16.10 mA/cm^2, a slightly improved FF of 68.7%, and delivers a best PCE of 10.06%. Finally, the N2200:PBDB-T based device exhibits a similar V_{oc} of 0.865 V, a slightly improved J_{sc} of 11.67 mA/cm^2, a similar FF of 66.1%, and a PCE of 6.65%. Analyzing these results, we can see that although both the ITIC and N2200 systems display enhanced absorption, only the ITIC:PBDB-T solar cell produces a PCE exceeding 10%, which can be attributed it to its largely improved J_{sc} value. The different photocurrents in these devices can be attributed to the different charge carrier properties in these systems. The external quantum efficiency (EQE) of these optimized PSC devices has been measured to evaluate the photoresponse as well as charge-collection efficiency. These results are shown in **Figure 2b**. We observe an overall increase in the EQE for both the ITIC and N2200 based devices in the absorbing region over 700 nm. This result displays the photocurrent contribution from the electron acceptors. However, this value significantly decreases in the N2200:PBDB-T based device, suggesting poor charge-collection efficiency at the longer wavelength. This deficiency can be attributed to the relatively low absorption coefficient of N2200 in the long-wavelength region.[26] Unexpectedly, the N2200:PBDB-T based device exhibits a slightly lower EQE value in the region between 400-700 nm compared to PCBM:PBDB-T, suggesting increased charge recombination in the N2200:PBDB-T cell. These *J*-*V* and EQE results demonstrate the benefits of nonfullerene acceptors in improving light-harvesting efficiencies in PSC devices.

To understand photovoltaic performance, charge transport is another crucial factor that must be understood.[27] The charge transporting properties in organic BHJ blends are normally characterized using the space-charge-limited current (SCLC) method.[28] This simple measurement is greatly influenced by the processing condition, thickness, morphology of the organic blend, and model applied to extract transport values. In this regard, SCLC characterization is undesired in fundamentally investigating the charge transporting properties of these blend films. Here, we conducted time-resolved microwave conductivity (TRMC) measurements.[29-30] TRMC is a contactless, optical pump-continuous microwave probe, technique that samples local free carrier mobility on the length scale of carrier delocalization. For intrinsic or fundamental investigations of charge carrier transport properties, TRMC is preferred because the measured mobility is minimally impacted by the types of bulk morphological non-uniformities that encumber long-range mobility measurements like SCLC. These include grain boundaries, bulk voids, and especially the charge extraction interfaces present in the device. As such, TRMC measurements give an indication of the potential performance, or the upper limit, that one could expect from a particular blend from a free carrier yield and mobility standpoint. Recently, Snaith et al. first explain the long-range charge carrier mobility in metal halide perovskite thin films using this technique.[31] As shown in **Figure 3a-b**, there are two primary figures of merit from the TRMC measurement: (i) the product ($\phi\sum\mu$) of the quantum efficiency of free carrier generation per photon absorbed (ϕ) and the sum of free electron and hole mobilities ($\sum\mu$), and (ii) the average free carrier lifetime (tau) extracted from the photoconductivity transient. Comparing the molecular acceptor blends, PCBM: PBDB-T exhibits a slightly higher $\phi\sum\mu$ than ITIC: PBDB-T (0.08 vs 0.06 cm^2 V^{-1} s^{-1}). Fullerenes are unique spheroid-shaped molecules that can form close contacts with each other and the donor in arbitrary directions, which can aid efficient charge transfer and delocalization as detected by TRMC.[31-32] However, the much lower absorption in visible and NIR regions of C_{60}-based fullerene derivatives severely limits their application in high-

efficiency PSCs. In contrast, the all-polymer blend N2200: PBDB-T exhibits the highest $\phi\sum\mu$ of 0.14 $cm^2\ V^{-1}\ s^{-1}$, nearly a two-fold increase over the molecular acceptor blends. Bi-exponential fits of the photoconductivity transients (**Figure 3b**), taken from the lowest absorbed flux points, reveal that the average free carrier lifetime is also highest in the N2200: PBDB-T blend (880 ns), resulting from fewer trap states and carrier recombination relative to both the PCBM: PBDB-T (760 ns) or ITIC: PBDB-T (630 ns) blends.[30]

With the experimentally determined yield-mobility product (μ) and carrier lifetime (τ) we can further evaluate the free charge carrier diffusion length (L_D) using the following equation:[33]

$$L_D = \sqrt{\tau \frac{\mu k_B T}{q}}$$

Where τ, μ, k_B, T, and q are charge carrier lifetime, charge mobility, Boltzmann constant, temperature, and elementary charge, respectively. Since the values here are derived from local properties, they also should serve as upper estimates of carrier diffusion, but nonetheless are quite useful to compare in the series. **Figure 3c** shows plots of each diffusion length relationship for a simulated range of ϕ values to demonstrate how $\phi\sum\mu$ values are deconvolved to calculate L_D. For each of the blends, a vertical dashed line indicates a separately measured IQE value (Figure S3, SI) corresponding to the same excitation wavelength as the TRMC measurement (640 nm). The N2200: PBDB-T blend (L_D=677 nm) exhibits a significantly longer free carrier diffusion length relative to the PCBM: PBDB-T (L_D=416 nm) and ITIC: PBDB-T (L_D=358 nm) blends. From this perspective the all-polymer blend is predicted to be a more desirable option for PSCs in terms of free charge generation, carrier mobility, and diffusion length. This prediction, based on local intrinsic properties, is in disagreement with our solar cell results, which necessitated additional analyses to understand this discrepancy by further examining the devices under operating conditions.

Numerous prior studies work have demonstrated that the charge transport process is strongly affected by the BHJ blend morphology.[17, 34] Therefore, a thorough morphological study may be helpful to understand the contradiction between the TRMC measurements and device performance. The morphology of the three optimal blend films were first examined by grazing-incidence wide-angle X-ray scattering (GIWAXS).[35] Two-dimensional (2D) scattering images and the corresponding line-cuts of blend films are shown in **Figures 4a-c** and Figures S4-S5, respectively. In all films, a diffraction peak corresponding to the π-π stacking structure appears along the q_z axis (out-of-plane direction), suggesting a preference for face-on orientation. As shown in Figure S4, the (010) diffraction peak of the acceptor appears in both the ITIC and N2200 based blends. A halo around 1.4 $Å^{-1}$ can be observed in the scattering spectra of PCBM: PBDB-T blend, which corresponds to a pure amorphous PCBM phase. Fullerenes are spherically symmetric materials which can have close contact with the donor molecules in arbitrary directions to achieve efficient charge transfer and transport.[36-38] The (010) diffraction peaks indicate a preference for face-on orientation for both PBDB-T and ITIC, which is beneficial for vertical charge transport in solar cell devices. In contrast, N2200: PBDB-T shows a strong π-π stacking diffraction peak in the out-of-plane direction as well as multiple diffraction peaks in the in-plane direction. Neat N2200 films have been widely reported to be high-crystalline films with strong face-on orientation.[39] Therefore, we hypothesized that there should be a crystallization competition between two conjugated polymers during the solution spin-coating process. Though the crystallization dynamics for each material during the blend film drying process have not been completely understood, we can conclude that the performance of all-polymer solar cells in large part depends on the morphology and optimization of the all-polymer blend. These morphologies are more complicated compared to both the PCBM and ITIC based blends.

To gain further insight into the phase separation and to confirm the GIWAXS results, we also investigated the film morphology through transmission electron microscopy (TEM),

as shown in **Figures 4d-f**. For the PCBM: PBDB-T blend, the donor polymer, and PCBM exhibits a phase separation scale around 10-20 nm, which is beneficial for carrier transport and efficient exciton dissociation.[17] The ITIC: PBDB-T blend shows similar features while with slightly larger ITIC domaina. Since ITIC is a more crystalline material compared to PCBM, it tends to aggregate in the solution-to-film transformation. Generally, both blend films exhibit a similar morphology which has been observed in previously reported efficient blend films. In contrast, N2200: PBDB-T shows very different blend morphology, as expected from the GIWAXS characterization. Such morphology included an apparent long-range ordered N2200 "wire" structure. The phase separation in the all-polymer blend is beyond the favorable nanoscale (~20 nm), which is theoretically not desired for exciton dissociation and would induce more charge recombination. Coupling the GIWAXS and TEM results, the all-polymer blend morphology may interpret the higher mobility, diffusion length, but lower photovoltaic performance in the all-polymer system.

Both the efficiency and stability of a solar cell is an essential consideration for practical applications.[40] Quite recently, PSCs have drawn lots of attention due to its excellent stability under both thermal stress and ambient conditions relative to PCBM or ITIC.[41-42] However, the reasoning behind these properties remains unclear. In this project, we finally systematically investigated the stability of these devices under the same operating conditions (Nitrogen (N_2) atmosphere without or with a continuous 80 °C thermal treatment). As shown in **Figure 5a**, all of these devices demonstrate a fairly stable performance in an inert atmosphere without encapsulation. After an initial minor decline in performance within the first 20 hours, the PCE remains steady and outputs over 90% of the initial performance during 300 hours of aging. Aging measurements were also carried out for devices under a continuous 80 °C thermal treatment. As shown in **Figure 5b**, only the N2200: PBDB-T cell was capable of maintaining stable performance under the thermal stress. Both the PCBM: PBDB-T and

ITIC: PBDB-T based devices deteriorate quickly and experience a PCE decay to ~60% of its

initial value within the first 10 hours. After the 10 hours, the PCE remained steady. It is also easy to correlate the stability to the morphology. Both the PCBM:PBDB-T and ITIC:PBDB-T exhibit a similar microstructure and phase separation scale. The thermal motion of molecules is more active in comparison to large-sized conjugated polymers. The unique all-polymer blends with a large D/A domain size has a higher tolerance to thermal stress. We conducted atomic force microscopy (AFM) measurements to confirm our prediction. As shown in Figure S6, the all-polymer blend exhibited stable morphological features under thermal stress compared to PCBM and ITIC based devices. Therefore, the relatively low efficiency and excellent device thermal stability for all-polymer solar cells can be a synergistic effect of the conjugated polymer itself and their current identical blend morphology.

3. Conclusion

In conclusion, through TRMC measurements we comparatively investigate the local intrinsic free-carrier properties in three representative organic BHJ blends. Such blends consist of a PBDB-T donor, two well-known molecular acceptors PCBM and ITIC, and polymeric acceptor N2200. We observe the best local free carrier generation and transport properties in the N2200: PBDB-T blend, which at the bulk scale produces an OPV device PCE around 6.65%. In contrast, the ITIC blend yields the lowest TRMC figures of merit and yet produces the overall best PCE amongst the acceptors, which exceeds 10%. By characterizing the bulk morphologies, we found that the properties of the long-range microstructure correlates best with the device results. The solar cell using either the PCBM or ITIC acceptor displays a more balanced donor and acceptor phase separation, leading to more efficient generation and transport of charges that can actually be collected in a working device. However, the more complex BHJ morphology formed in all-polymer blends, we suppose due to donor and acceptor chain entanglement as well as secondary and tertiary packing motifs in both phases, in fact delivers a more thermally stable morphology in the operating device. We

believe that the results presented here are important in understanding and improving the efficiency and stability of organic solar cells, especially since new high-performance classes of acceptor materials clearly induce BHJ morphologies that may trade-off reaching their intrinsic performance potential for operational thermal stability in the device.

Experimental Section

Materials: PBDB-T (M_w>100.0 kg/mol, PDI <3.0), PCBM and ITIC were purchased from 1-Materials Inc. N2200 was synthesized according our previous report (M_n = 36.0 kg/mol, PDI = 2.5).[43]

Time-Resolved Microwave Conductivity: The sample is placed in a microwave cavity at the end of an X-band waveguide operating at ca. 9 GHz, and is photoexcited through a grid with a 5 ns laser pulse from an OPO pumped by the third harmonic of an Nd:YAG laser. The relative change of the microwave power, P, in the cavity, due to absorption of the microwaves by the photoinduced free electrons and holes, is related to the transient photoconductance, ΔG, by $\Delta P/P = -K\Delta G$, where the calibration factor K is experimentally determined individually for each sample. Taking into account that the electrons and holes are generated in pairs, the peak photoconductance during the laser pulse can be expressed as: $\Delta G = \beta q_e F_A I_0 (\varphi \cdot \Sigma\mu)$. where q_e is the elementary charge, β=2.2 is the geometric factor for the X-band waveguide used, I_0 is the incident photon flux, F_A the fraction of light absorbed at the excitation wavelength, φ is the quantum efficiency of free carrier generation per photon absorbed and Σμ the sum of the mobilities of electrons and holes. The equation is used to evaluate the quantum efficiency or free carrier generation per photon absorbed, multiplied by the local mobility of free carriers. These quantities can often be correlated with molecular structure to provide insight into the mechanisms for free carrier generation and transport in all-polymer composites as a function of the microstructure. The photoconductance decay after the end of the laser pulse is also a useful tool for the characterization of free carrier decay mechanisms by recombination and

trapping. Active layer blend samples for this work were prepared on quartz substrates according to an optimized device conditions.

Supporting Information
Supporting Information is available from the Wiley Online Library or from the author.

Acknowledgements

This work was supported by the Natural Science Foundation of Jiangsu Province of China (BK20170337), the National Natural Science Foundation of China (Grant No. 51803144, 51761145013 and 61674111), China Postdoctoral Science Foundation (Grant No. 2019M651942), and "111" projects. The author thanks the Collaborative Innovation Center of Suzhou Nano Science and Technology, Soochow University, the Priority Academic Program Development of Jiangsu Higher Education Institutions (PAPD). This work was authored in part by the National Renewable Energy Laboratory, operated by Alliance for Sustainable Energy, LLC, for the U.S. Department of Energy (DOE) under Contract No. DE-AC36-08GO28308. Microwave conductivity measurements were funded through the Office of Energy Efficiency and Renewable Energy Solar Energy Technologies Office. The views expressed in the article do not necessarily represent the views of the DOE or the U.S. Government. The U.S. Government retains and the publisher, by accepting the article for publication, acknowledges that the U.S. Government retains a nonexclusive, paid-up, irrevocable, worldwide license to publish or reproduce the published form of this work, or allow others to do so, for U.S. Government purposes. The use of the Advanced Light Source beamline 7.3.3 for grazing incidence wide angle X-ray scattering, beamline 11.0.1.2 for resonant soft X-ray scattering, and beamline 6.3.2 for near edge X-ray absorption fine structure spectroscopy are supported by the Director, Office of Science, Office of Basic Energy Sciences, of the DOE under contract no. DE-AC02-05CH11231.

Received: ((will be filled in by the editorial staff))
Revised: ((will be filled in by the editorial staff))
Published online: ((will be filled in by the editorial staff))

References

1. G. Yu, J. Gao, J. C. Hummelen, F. Wudl, A. J. Heeger, *Science* **1995**, *270*, 1789.
2. Y. Li, *Acc. Chem. Res.* **2012**, *45*, 723.
3. J. Hou, O. Inganäs, R.H. Friend, F. Gao, *Nat. Mater.,* **2018**, *17*, 119.
4. P. Cheng, G. Li, X. Zhan, Y. Yang, *Nat. Photonics,* **2018**, *12*, 131.
5. Z. Zhang, H.S. Tan, X. Guo, A. Facchetti, H. Yan, *Nat. Energy,* **2018**, *3*, 720.
6. Cheng, Y.-J.; Yang, S.-H.; Hsu, C.-S. *Chem. Rev.* **2009**, *109*, 5868.
7. H. Yao, L. Ye., H. Zhang, S. Li, S. Zhang, J. Hou, *Chem. Rev.*, **2016**, *116*, 7397.
8. Y. Liu, J. Zhao, Z. Li, C. Mu, W.; Ma, H. Hu, K. Jiang, H. Lin, H. Ade, H. Yan, *Nat.*

Commun. **2014**, *5*, 5293.

9. Z. He, B. Xiao, F. Liu, H. Wu, Y. Yang, S. Xiao, C. Wang, T. P. Russell, Y. Cao, *Nat. Photonics* **2015**, *9*, 174.
10. J. Yuan, Y. Zhang, L. Zhou, G. Zhang, H.-L. Yip, T.-K. Lau, X. Lu, C. Zhu, H. Peng, P. A. Johnson, M. Leclerc, Y. Cao, J. Ulanski, Y. Li, Y. Zou, *Joule,* **2019**, *3*, 1140.
11. Y. Cui, H. Yao, J. Zhang, T. Zhang, Y. Wang, L. Hong, K. Xian, B. Xu, S. Zhang, J. Peng, Z. Wei, F. Gao, J. Hou *Nat. Commun.*, 2019, *10*, 2515.
12. A. Facchetti, *Mater. Today* **2013**, *16*, 123.
13. T. Kim, J. H. Kim, T. E. Kang, C. Lee, H. Kang, M. Shin, C. Wang, B. Ma, U. Jeong, T. S. Kim, B. J. Kim, *Nat. Commun.* **2015**, *6*, 8547.
14. Y. Zhang, Y. Xu, M. J. Ford, F. Li, J. Sun, X. Ling, Y. Wang, J. Gu, J. Yuan, W. Ma, *Adv. Energy Mater.* **2018**, *8*, 1800029.
15. W. Zhao, D. Qian, S. Zhang, S. Li, O. Inganäs, F. Gao, J. Hou, *Adv. Mater.* **2016**, *28*, 4734.
16. Y. Xu, J. Yuan, S. Zhou, M. Seifrid, L. Ying, B. Li, F. Huang, G. C. Bazan, W. Ma, *Adv. Funct. Mater.* **2019**, *28*, 1806747.
17. Y. Huang, E. J. Krammer, A. J. Heeger, G. C. Bazan, Chem. Rev. **2014**, *114*, 7006;
18. J. K. Lee, W. L. Ma, C. J. Brabec, J. S. Moon, J. Y. Kim, K. Lee, G. C. Bazan, A. J. Heeger, *J. Am. Chem. Soc.* **2008**, *130*, 3619.
19. J. Yuan, Y. Xu, G. Shi, X. Ling, L. Ying, F. Huang, T. H. Lee, H. Y. Woo, J. Y. Kim, Yong Cao, W. Ma, *J. Mater. Chem. A* **2018**, *6*, 10421.
20. Y. Lin, J. Wang, Z. G. Zhang, H. Bai, Y. Li, D. Zhu, X. Zhan, *Adv. Mater.*, **2015**, *27*, 1170.
21. K. Zhang, R. Xia, B. Fan, X. Liu, Z. Wang, S. Dong, H.-L. Yip, L. Ying, F. Huang, Y. Cao, *Adv. Mater.* **2018**, *30*, 1803166.
22. B. Fan, L. Ying, Z. Wang, B. He, X.-F. Jiang, F. Huang, Y. Cao, *Energy Environ. Sci.* **2017**, *10*, 1243.
23. L. Zhu, W. Zhong, C. Qiu, B. Lyu, Z. Zhou, M. Zhang, J. Song, J. Xu, J. Wang, J. Ali, W Feng, Z. Shi, X. Gu, L. Ying, Y. Zhang, Feng Liu, *Adv. Mater.*, **2019**, *31*, 1902899.
24. H. Yan, Z. Chen, Y. Zheng, C. Newman, J.R. Quinn, F. Dotz, M. Kastler, A. Facchetti, *Nature* **2009**, *457*, 679.
25. W. Zhao, S. Li, H. Yao, S. Zhang, Y. Zhang, B. Yang, J. Hou, *J. Am. Chem. Soc.*, **2017**, *139*, 7148.
26. Z. Li, X. Xu, W. Zhang, X. Meng, W. Ma, A. Yartsev, O. Inganäs, M. R Andersson, R A.

J. Janssen, E. Wang, *J. Am. Chem. Soc.* **2016**, *138*, 10935.
27. C.M. Proctor, M. Kuik, T.-Q. Nguyen, *Prog. Polym. Sci.* **2016**, *38*, 1941.
28. A. Rose, *Phys. Rev.* **1955**, *97*, 1538.
29. L. E. Garner, A. Bera, B. W. Larson, D. P. Ostrowski, A. J. Pal, W. A. Braunecker, *ACS Energy Lett.* **2017**, *2*, 1556.
30. Y. Xu, J. Yuan, S. Liang, J.-D. Chen, Y. Xia, B. W. Larson, Y. Wang, G. M. Su, Y. Zhang, C. Cui, M. Wang, H. Zhao, W. Ma *ACS Energy Lett.* **2019**, *4*, 2277.
31. A. M. Nardes , A. J. Ferguson , J. B. Whitaker, B. W. Larson, R. E. Larsen, K. Maturová, P. A. Graf, O. V. Boltalina, S. H. Strauss, N. Kopidakis, *Adv. Funct. Mater.* **2012**, *22*, 4115.
32. B. W. Larson, O. G. Reid, D. C. Coffey, S. M. Avdoshenko, A. A. Popov, O. V. Boltalina, S. H. Strauss, N. Kopidakis, G. Rumbles, *Adv. Energy Mater.* **2016**, *6*, 1601427.
33. J. Lim, M. T. Horantner, N. Sakai, J. M. Ball, S. Mahesh, N. K. Noel, Y.-H.Lin, J. B. Patel, D. P. McMeekin, M. B. Johnston, B. Wenger, H. J. Snaith, *Energy Environ. Sci.* **2019**, *12*, 169.
34. B. C. Thompson, J. M. J. Fréchet, *Angew. Chem. Int. Ed.* **2008**, *47*, 58.
35. J. Rivnay, S. C. B. Mannsfeld, C. E. Miller, A. Salleo, M. F. Toney, *Chem. Rev.* **2012**, *112*, 5488.
36. M. Schubert, B.A. Collins, H. Mangold, I.A. Howard, W. Schindler, K. Vandewal, S. Roland, J. Behrends, F. Kraffert, R. Steyrleuthner, Z. Chen, K. Fostiropoulos, R. Bittl, A. Salleo, A. Facchetti, F. Laquai, H. Ade, D. Neher, *Adv. Funct. Mater.*, **2014**, *24*, 4068.
37. Y. Li, Y. Zhou, *Adv. Mater.*, **2008**, *20*, 2952.
38. J. Yuan, W. Guo, Y. Xia, M.J. Ford, F. Jin, D. Liu, H. Zhao, O. Inganäs, G.C. Bazan, W. Ma, *Nano Energy* **2017**, *35*, 251.
39. S. Holliday, R. S.Ashraf, A. Wadsworth, D. Baran, S. A. Yousaf, C. B. Nielsen, C.-H. Tan, S. D. Dimitrov, Z. Shang, N. Gasparini, M. Alamoudi, F. Laquai, C. J. Brabec, A. Salleo, J. R. Durrant, I. McCulloch, *Nat. Commun.* **2016**, *7*, 11585.
40. M. Jørgensen, K. Norrman, F. C. Krebs, *Sol. Energy Mater. Sol. Cells*, **2008**, *92*, 686.
41. C. Lee, S. Lee, G.-U. Kim, W. Lee, B. J. Kim, *Chem. Rev.* **2019**, *119*, 8028.
42. Z. Li, W. Zhang, X. Xu, Z. Genene, D. Di Carlo Rasi, W. Mammo, AYartsev, M. R. Andersson, RA. J. Janssen, EWang, *Adv. Energy Mater.* **2017**, *7*, 1602722.
43. J. Yuan, W. Ma J. Mater. Chem. A, **2015**, *3*, 7077.

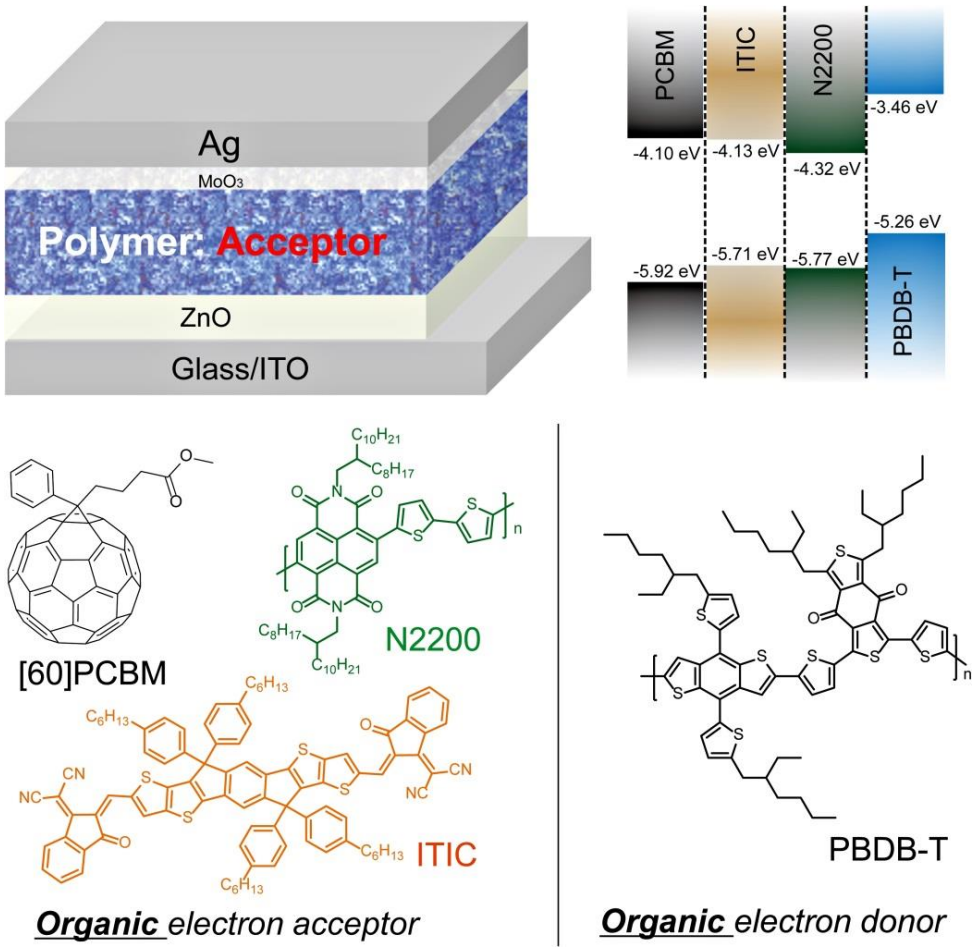

Figure 1. Schematic illustration of the device structure of inverted BHJ polymer solar cells together with the energy levels and chemical structure of PBDB-T, PCBM, ITIC and N2200.

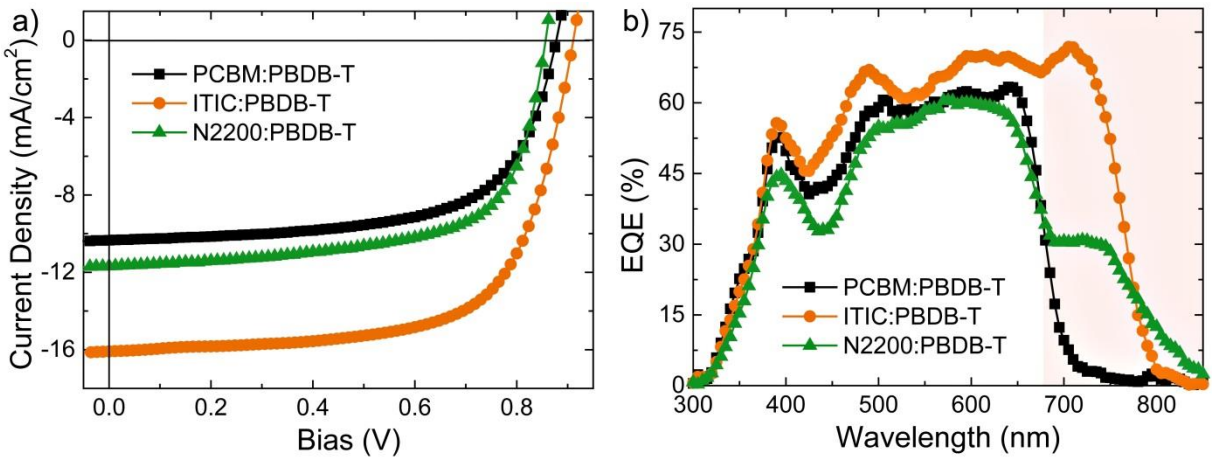

Figure 2. Current–voltage characteristics (a) under AM 1.5G, 100 mW cm^{-2} and EQE (b) of optimized polymer solar cell devices based on different electron acceptors, respectively.

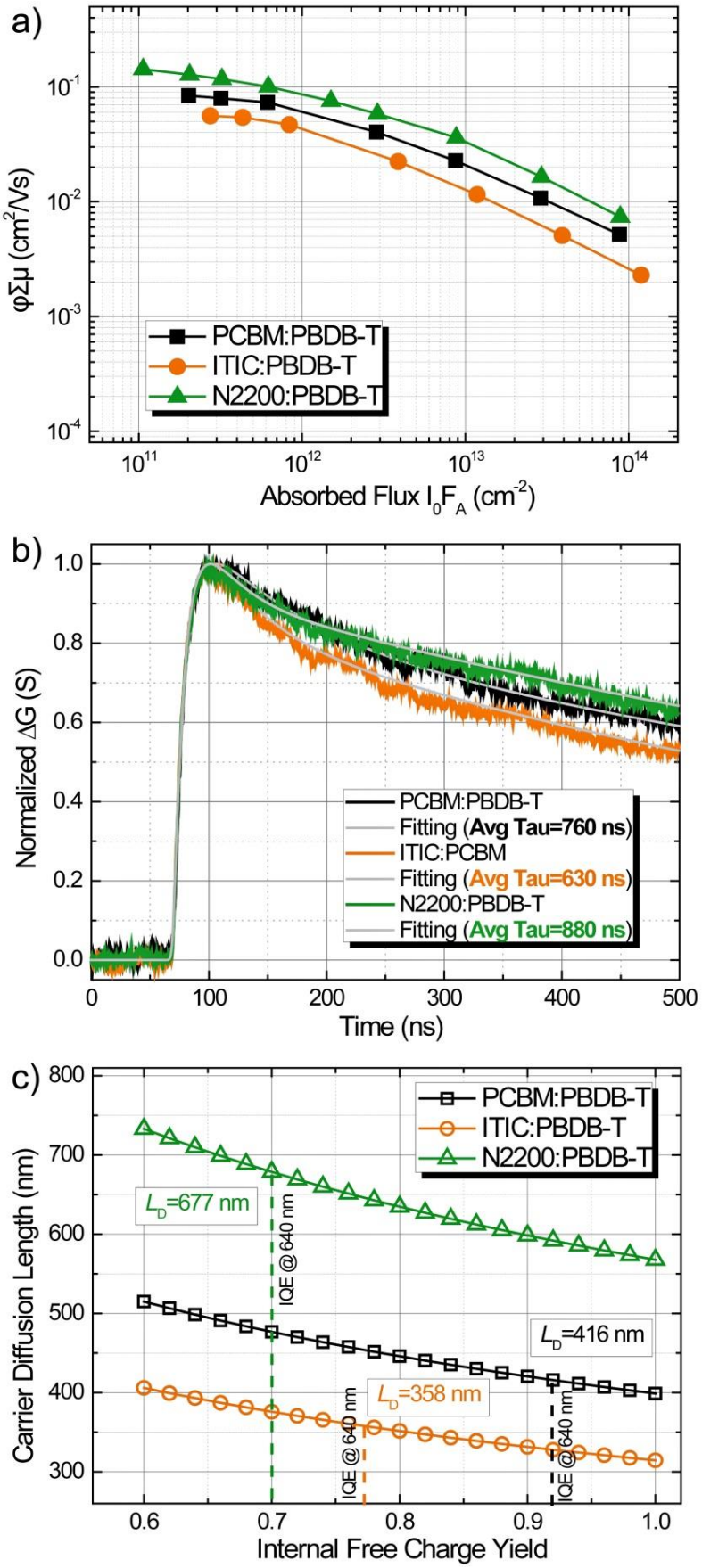

Figure 3. (a) The product of charge carrier yield (ϕ) and sum of free carrier mobilities (Σμ), and (b) TRMC transients (b) for BHJ PBDB-T: electron acceptor blends at a laser excitation wavelength of 640 nm. (c) Calculated free carrier diffusion length.

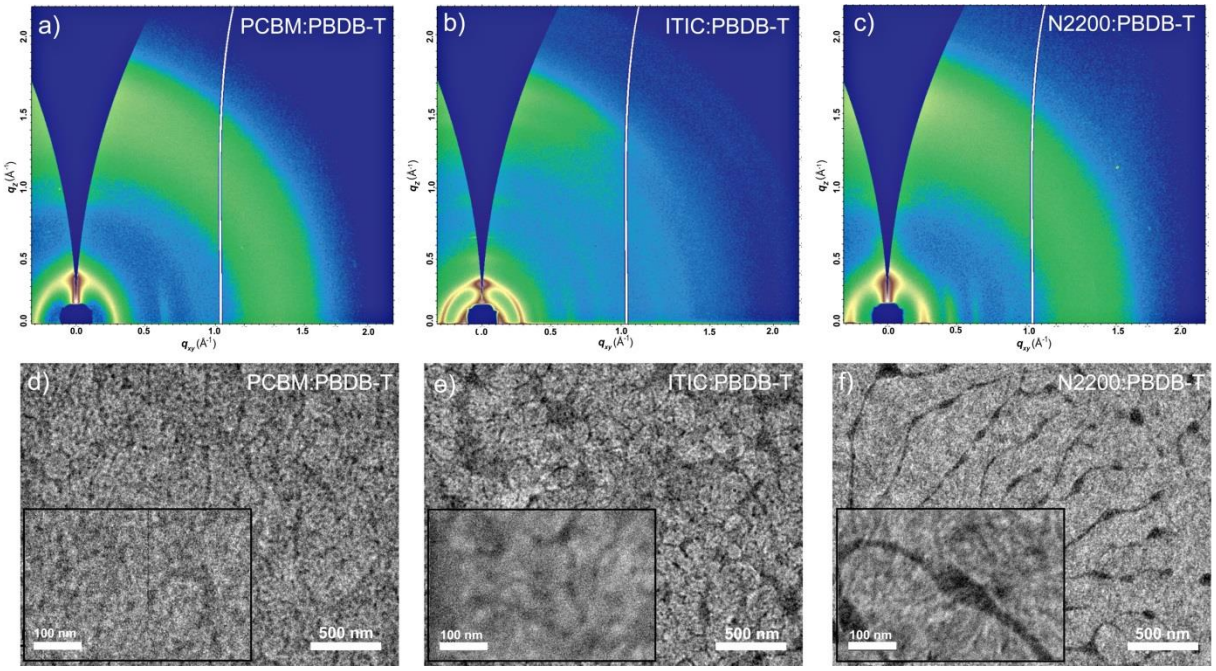

Figure 4. Two-dimensional GIWAXS diffraction patterns of PCBM:PBDB-T (a), ITIC:PBDB-T (b) and N2200:PBDB-T blend films (c); TEM images at different scale of PCBM:PBDB-T (d), ITIC:PBDB-T (e) and N2200:PBDB-T blend films (f).

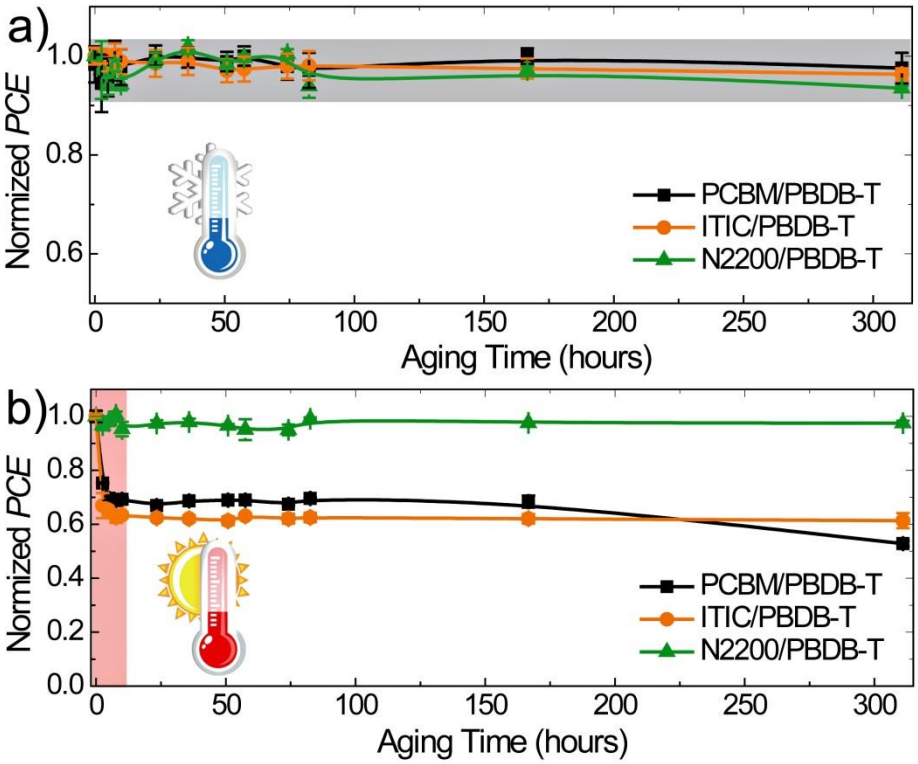

Figure 5. Thermal stability of polymer solar cell devices based on different electron acceptors kept in room temperature (a) and on the hotplate at 80 °C (b) in N_2-filled glovebox.

Table 1. Device parameters of PBDB-T based polymer solar cells.

Acceptor	V_{oc} (V)	J_{sc} (mA/cm^2)	FF (%)	PCE (%)	Yield Mobility Product (cm^2 V^{-1}s^{-1})	TRMC Lifetime (ns)	Free Carrier Diffusion Length (nm)
PCBM	0.875	10.34	65.1	5.88	0.08	760	416
ITIC	0.910	16.10	68.7	10.06	0.06	630	358
N2200	0.865	11.67	66.1	6.65	0.14	880	677

Through time-resolved microwave conductivity (TRMC) measurements, we comparatively investigate the local intrinsic free-carrier properties in three representative organic BHJ blends, and we believe that the results presented here are important in understanding and improving the efficiency and stability of organic solar cells.

Keyword: polymer solar cells, nonfullerene acceptor, time-resolved microwave conductivity (TRMC), free carrier mobility, stability

*Qilin Zhang, Xin Yuan, Yifeng Feng, Bryon W. Larson, Gregory M. Su, Yin Maung Maung, Nopporn Rujisamphan, Youyong Li, Jianyu Yuan, * Wanli Ma**

Understanding the interplay of transport-morphology-performance in PBDB-T based polymer solar cells

ToC:

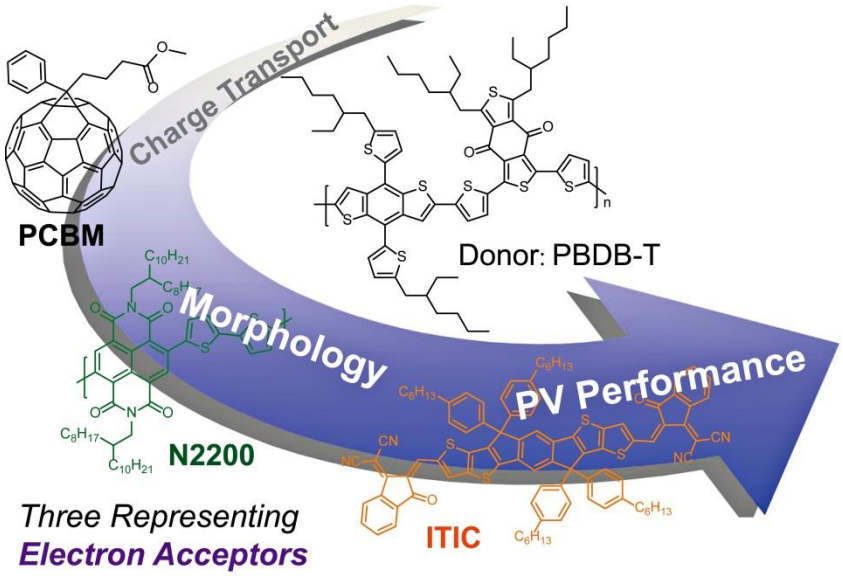

Supporting Information

Understanding the interplay of transport-morphology-performance in PBDB-T based polymer solar cells

*Qilin Zhang, Xin Yuan, Yifeng Feng, Bryon W. Larson, Gregory M. Su, Yin Maung Maung, Nopporn Rujisamphan, Youyong Li, Jianyu Yuan, * Wanli Ma**

Qilin Zhang, Xin Yuan, Yifeng Feng, Prof. Youyong Li, Prof. Jianyu Yuan, Prof. Wanli Ma
Institute of Functional Nano & Soft Materials (FUNSOM), Jiangsu Key Laboratory for Carbon-Based Functional Materials and Devices, Joint International Research Laboratory of Carbon-Based Functional Materials and Devices, Soochow University, Suzhou, 215123, P. R. China

Dr. Bryon W. Larson
Chemistry & Nanoscience Department, National Renewable Energy Laboratory, Golden, Colorado 80401, United States

Dr. Gregory M. Su
Advanced Light Source, Lawrence Berkeley National Laboratory, Berkeley, California 94720, United States

Prof. Yin Maung Maung,
Department of Physics, University of Yangon, Pyay Road, Yangon 11181, Myanmar

Prof. Nopporn Rujisamphan
King Mongkut's University of Technology Thonburi (KMUTT), 126 Pracha Uthit Road, Bang Mod, Thung Khru, Bangkok 10140, Thailand

Keywords: polymer solar cells, nonfullerene acceptor, time-resolved microwave conductivity (TRMC), free carrier mobility, stability

1. Characterization

UV-vis-NIR spectrums were recorded on a Perkin Elmer model Lambda 750. UPS measurements were performed using an Omicron Nanotechnology system with a base pressure of 2.0×10^{-10} Torr. GIWAXS measurements were performed at the Advanced Light Source (ALS)-Lawrence Berkeley National Laboratory on Beamline 7.3.3. Atomic force microscopy (AFM) and transmission electron microscopy (TEM) images were captured using a Veeco Multimode V instrument and Tecnai G2 F20 S-Twin transmission electron microscope, respectively. The external quantum efficiency (EQE) was performed using a certified IPCE instrument (Zolix Instruments, Inc, SolarCellScan100).

2. Device Fabrication and Measurements:

The structure of all-polymer soar cells was ITO/ZnO/blend/MoO_3/Ag, which can be found in our previous report. For the bulk heterojunction devices, PBDB-T:N2200 all-polymer blend solutions (8 mg/mL, D/A ratio=2/1) in chlorobenzene were kept heating at 40 ^oC for at least 6 h. All-polymer active layer was spin-coated onto the top of ZnO layer at 2500 rpm for 60 s, which was further were thermally annealed at varying temperatures for 10 min in glovebox. For the planar heterojunction devices, neat N2200 layer was spin-coated onto the top of ZnO using varying polymer concentration (2 mg/mL to 8 mg/mL) at 2000 rpm for 60 s to achieve different thickness, and then PBDB-T solution in chloroform was quickly drop on top of N2200 layer and was spin-coated at 2000 rpm for 40 s with varying polymer concentration (2 mg/mL to 6 mg/mL). The optimized condition for planar all-polymer devices: N2200 in chlorobenzene (4 mg/mL) spin-coated at 2000 rpm 40s to obtain a thickness ~60 nm, and then PBDB-T (chloroform 4 mg/mL) on top spin-coated at 2000 rpm for 40s to obtain a thickness ~50 nm. The planar all-polymer devices were also thermally annealed at varying temperatures for 10 min in glovebox. Finally, MoO_3 at a speed of 0.2 Å/s

(9.0 nm), and anode Ag at a speed of 2 Å /s (100 nm) layers were then thermally evaporated according to our previous method.[37] The protocol for solar cells characterization (J-V characteristics, EQE) was according to our previous report.[37] Solar cell devices were measured in forward scan (-1.0 V → 1.0 V, step 0.0125 V, scan rate: 0.1 V s^{-1}) without an illumination mask in glovebox. The stabilized PCE value was taken for each device.

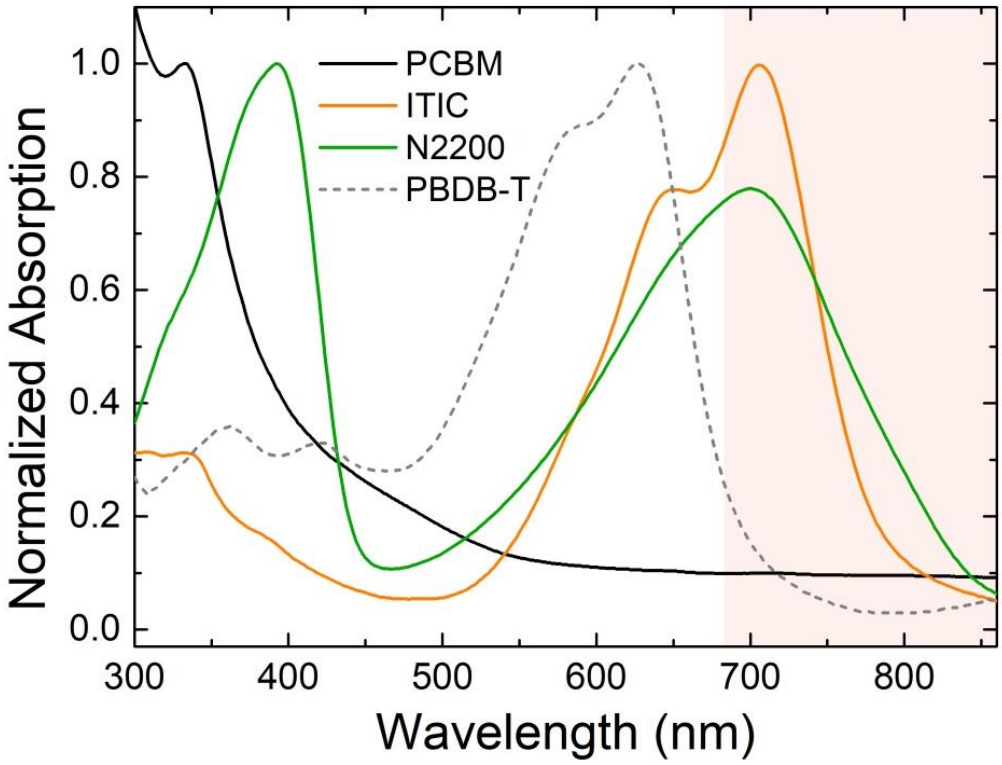

Figure S1. UV-vis absorption spectra of PBDB-T and different electron acceptors

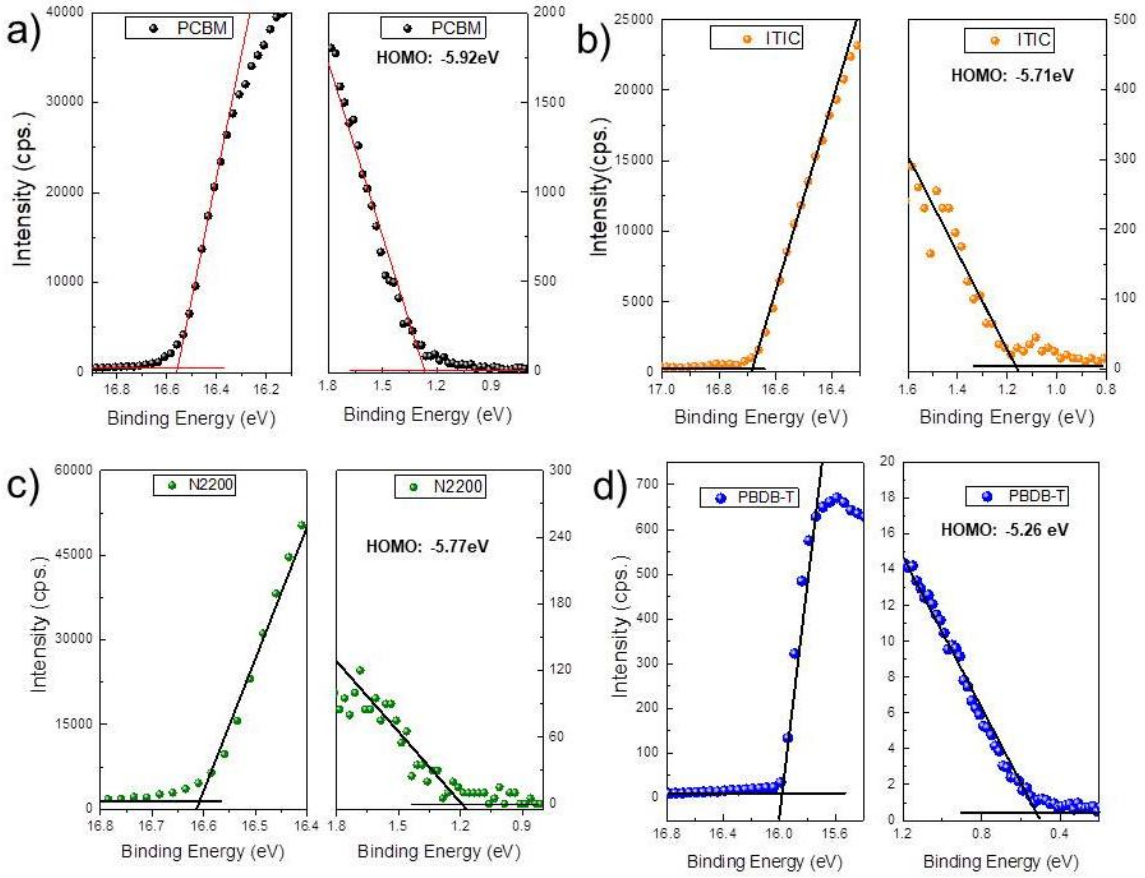

Figure S2. UPS spectra of PCBM (a), ITIC (b) and N2200 (c) and PBDB-T (d) film.

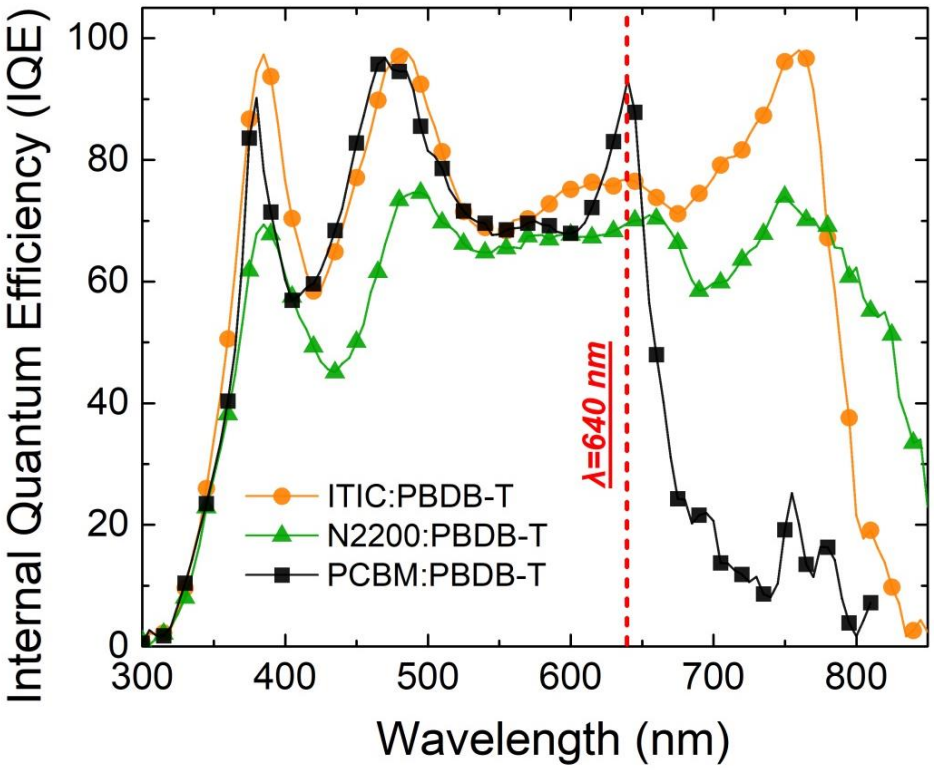

Figure S3. IQE of optimized polymer solar cell devices based on different electron acceptors, respectively.

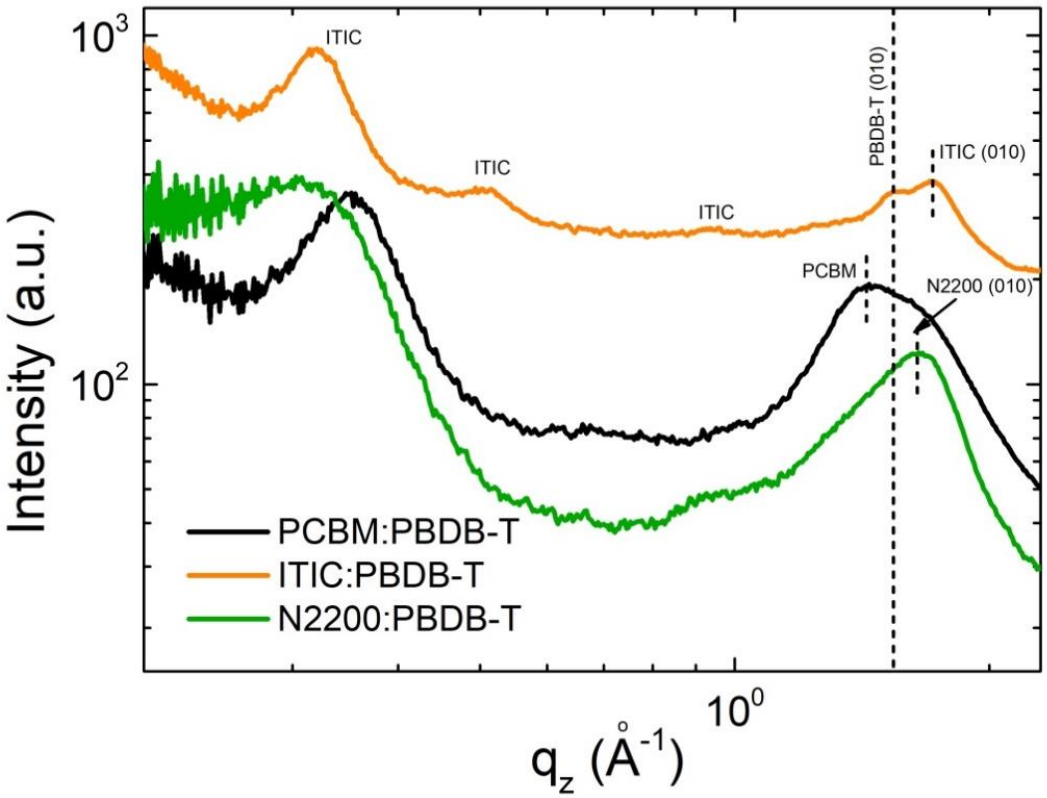

Figure S4. Out-of-plane line cuts of the corresponding 2D GIWAXS images.

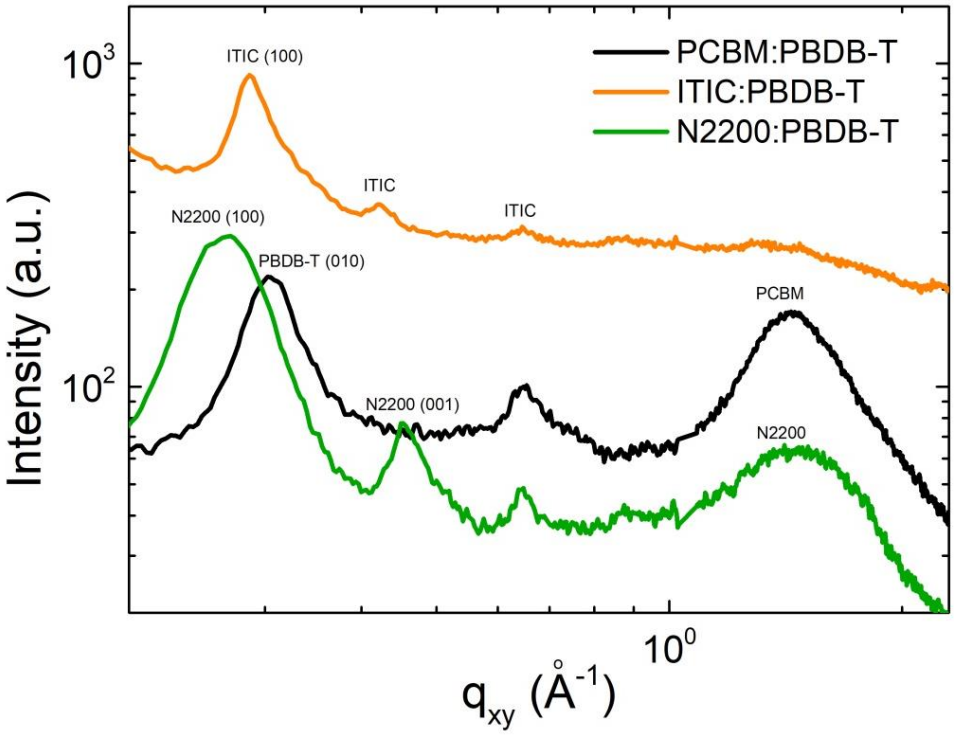

Figure S5. In-plane line cuts of the corresponding 2D GIWAXS images.

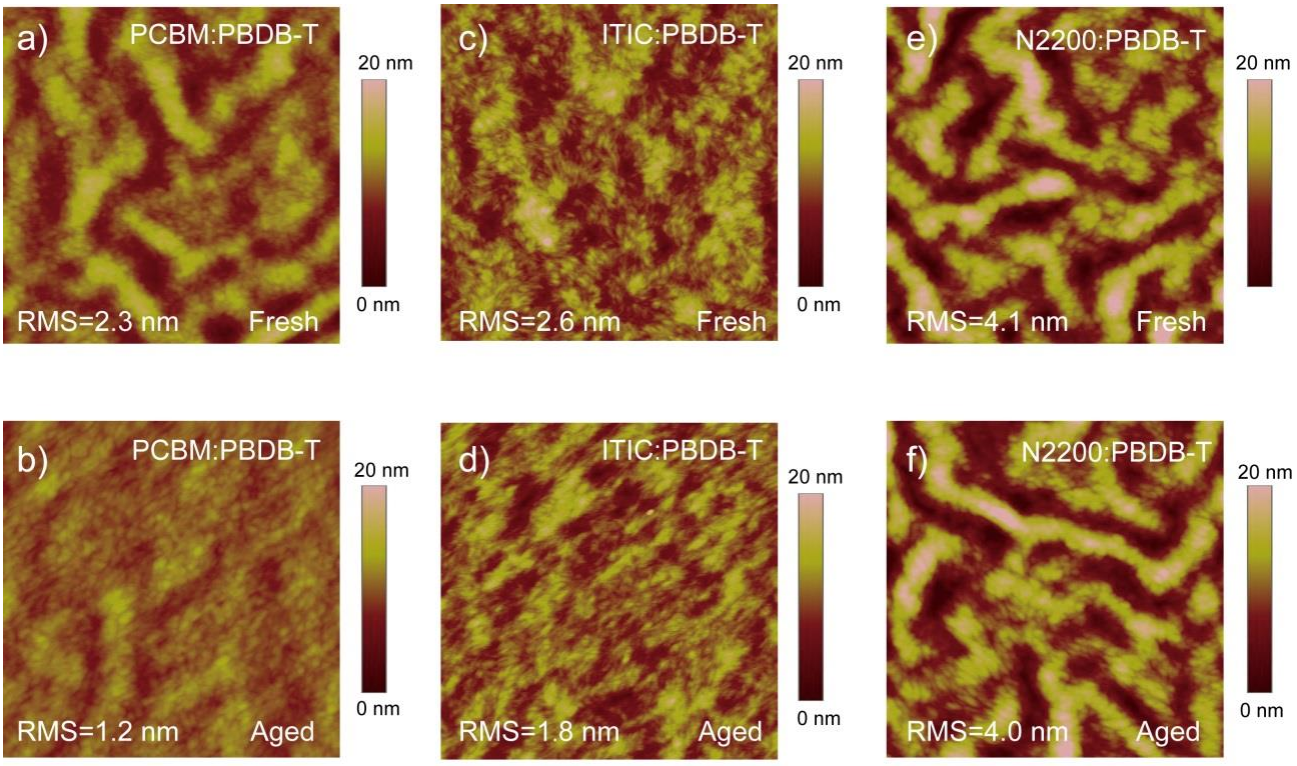

Figure S6. AFM images of fresh and agend PCBM:PBDB-T (a, b), ITIC:PBDB-T (c, d) and N2200:PBDB-T blend films (e, f).